THE EVALUATION OF DROP SIZE DISTRUBUTIONS CAPTURED BY TWO WEATHER RADARS IN MID MISSOURI

A Thesis

presented to

the Faculty of the Graduate School

at the University of Missouri-Columbia

In Partial Fulfillment

of the Requirements for the Degree

Master of Science

By

MOSES FARR

Dr. Neil Ian Fox, Thesis Supervisor

DECEMBER 2022

The undersigned, appointed by the dean of the Graduate School, have examined the thesis entitled

THE EVALUATION OF DROP SIZE DISTRUBUTIONS CAPTURED BY TWO WEATHER RADARS IN MID MISSOURI

presented by Moses Farr,

a candidate for the degree of Master of Science

and hereby certify that, in their opinion, it is worthy of acceptance

_____

Professor Neil Fox

_____

Professor Noel Aloysius

_____

Professor Adam Helfer

AKNOWLEDGEMENTS

I would like to thank all of my professors who have offered their wisdom and knowledge throughout my academic career. I would like to specifically thank my thesis committee, whose guidance has been extremely helpful throughout the drafting of this document. A special thanks of gratitude goes to PhD candidate, Christopher Stewart, who helped draft much of the coding that was used in the analysis of the data processed.

TABLE OF CONTENTS

LIST OF FIGURES

LIST OF TABLES

ABSTRACT

In 2015, an X-band dual-polarization Doppler radar (MZZU) was installed in Columbia, Missouri. Its goal is to fill a gap in radar coverage and provide a precipitation climatology for Mid-Missouri. MZZU captures precipitation data by transmitting frequencies at 9.35 GHz. During heavy rainfall events, however, the power of the emitted X-band waves is attenuated. Currently, an attenuation correction algorithm is processing MZZU data to improve the accuracy of the radar. This study uses a K-band vertical pointed microwave rain radar (MRR) to evaluate the need to further calibrate MZZU data. Eight events were analyzed and the correlation of attenuated corrected reflectivity from MZZU and reflectivity from the MRR were calculated. The correlation of reflectivity values was 0.77 with a RMSE of 4.73 dBZ in all elevations. MZZU underestimated reflectivity values with an average negative bias of 7.71 dBZ. A linear regression line was fitted as well with slope values ranging from 0.61-0.71. Specifically in events with moderate rainfall, the correlation improved with R^2 values greater than 0.9; however, the bias increased to 11.68 dBZ. This suggests that radome attenuation may be resulting in higher biases in moderate rain events. In all events and elevations, MZZU underestimated reflectivity compared to the MRR. However, the values obtained from the linear relationship between MZZU and the MRR may be used in future studies to calibrate MZZU reflectivity values.

1. INTRODUCTION

1.1. Research Impacts

Qualitative precipitation estimates (QPEs) provide meteorologists with the resources to create hazardous weather outlooks. In Mid-Missouri, the lack of radar coverage from the Next-Generation Radar network (NEXRAD) makes it difficult to obtain accurate QPEs for the region. MZZU, an X-band dual-polarization Doppler radar, was installed to help fill this gap, but its high frequency output leads to attenuation during heavy rain periods. Heavy rainfall can lead to short-lived, localized floods known as flash floods (Rauber, Walsh and Charlevoix 2017). Flash flooding is responsible for the largest number of fatalities among severe weather hazards. Missouri ranks the 8th state with most flood fatalities in the continental United States (Ashley and Ashley 2008).

Due to attenuation during heavy rain events, rainfall rates calculated from MZZU reflectivity values are greatly underestimated. If reflectivity values from MZZU can be improved, then meteorologists can produce more accurate rainfall estimates. These improved QPEs allow meteorologists to post flash flood watches and warnings sooner, resulting in more lives saved. Therefore, the goal of this study is to improve the reflectivity values received from MZZU by using drop size distribution (DSD) retrievals obtained from a K-band vertical pointed microwave rain radar (MRR). MRRs have been used to calibrate X-Band radars in previous studies. However, DSDs vary by location due to climatological and microphysical factors. Thus, an analysis of the DSD retrievals from MZZU and the MRR provide important information about precipitation in Mid-Missouri.

1.2. Quantitative Precipitation Estimations from Radar

Weather radars sense hydrometeorological data that is then used in operational meteorology and meteorological research. A radar collects data by sending out electromagnetic (EM) waves that interact with particles in the atmosphere. These particles generate their own EM waves as a result, and the radar senses the back-scattered radiation. Specifically, weather radars measure the power of the return signal by using the standard form of the radar equation as presented by Ryzhkov and Zrnic (2019):

$$P_h = \left(\frac{\pi^3 P_h^t g^2 c\tau\theta_1^2}{2^{10} ln\, 2\lambda^2 l_r}\right)\frac{|K_w|^2}{r_0^2 l_h^2} Z_h \quad (1)$$

where P_h is the received signal power and Z_h is the equivalent reflectivity factor in a horizontal polarization configuration.

The equivalent reflectivity factor, commonly referred to as reflectivity (Z), is one of the earliest products measured by weather radars. Marshall and Palmer (1948) formulated the equation

$$Z = 200R^{1.6} \quad (2)$$

where Z is the equivalent reflectivity factor measured in $mm^6\ m^{-3}$ and R is the rainfall rate in $mm\ h^{-1}$. The Marshall and Palmer equation relates the reflectivity sensed by the radar to the rainfall rate and is still commonly used today in meteorological practice. Qualitative precipitation estimates (QPE) of the rainfall rate allow meteorologists to forecast advanced warnings, specifically in regard to severe thunderstorms.

1.3. Drop Size Distributions

In Eq. (1), the equivalent reflectivity factor is calculated using the equation:

$$Z = \int_0^\infty N(D)D^6 dD \quad (3)$$

where Z is the equivalent reflectivity factor and $N(D)$ is the concentration of drops of size D where D is the diameter. The combination of $N(D)$ and D help define the drop size distributions (DSDs) within storms. The variability of DSDs in different rain events has huge impacts on the equivalent reflectivity factor sensed by the radar. This is the result of microphysical factors in which raindrops form.

In a scenario where cloud droplets develop below the freezing level, an updraft of moisture leads to the condensation of water vapor in the atmosphere. These drops grow in size until the saturation vapor pressure reaches equilibrium. Once the updraft is no longer able to suspend the cloud droplets, they begin to fall. The raindrops will then collide and coalesce as they descend due to the horizontal and vertical components of the wind. The wind will also sort drops based on their size as smaller drops are influenced more by wind than larger drops. Thus, larger drops grow at the expense of smaller drops. In general, an increase in drop diameter will lead to the decrease in drop concentration (Schuur, Ryzhkov and Clabo 2005).

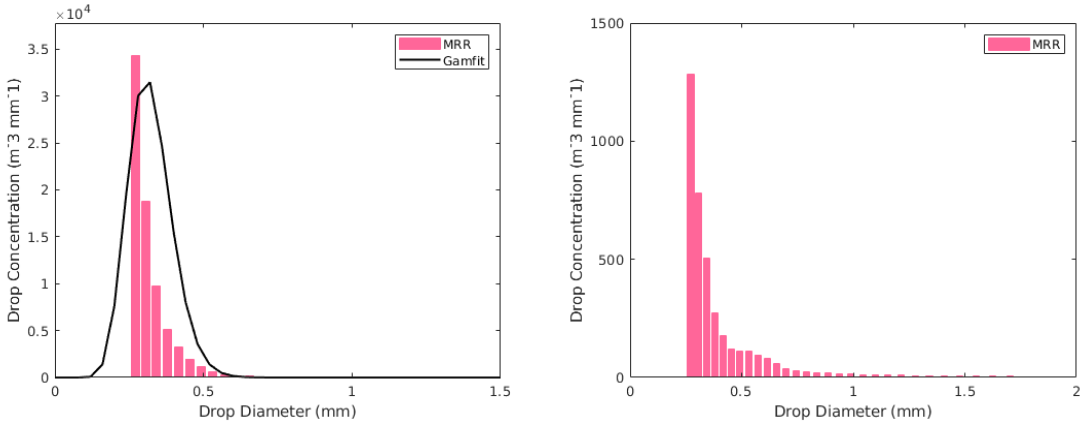

Figure 1. DSDs from a stratiform event (Left) and a convective event (Right). The gamma fit model is plotted on the left.

As shown in Eq. (3), reflectivity is calculated using the sixth moment of the drop diameter. Therefore, one 5 mm drop generates the same reflectivity factor as one million 0.5 mm drops. In operational meteorology, reflectivity is expressed in logarithmic units of decibels (dBZ) where:

$$dBZ = 10\,log(Z) \tag{4}$$

In moderate rain events where convection is limited, the concentration of smaller drops is high and drop sizes are more evenly distributed (Figure 1). The reflectivity values in stratiform events typically range from 30-40dBZ, while values in convective events range from 40-65 dBZ (Figure 2). The drop size distributions in heavy rain events are more chaotic due to strong updrafts, which leads to a higher concentration of larger drops. Therefore, the National Weather Service (NWS) uses multiple R(Z) equations to account for different DSDs depending on storm type (Table 1).

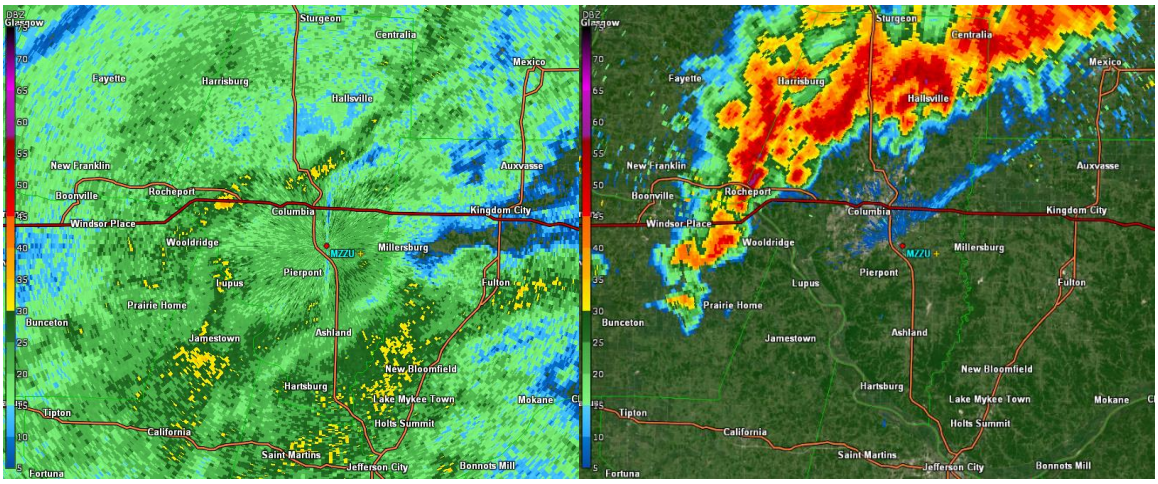

Figure 2. Reflectivity values retrieved from a stratiform event (Left) and a convective event (Right) by MZZU. Reflectivity is displayed using the GR2Analyst software.

Table 1. List of $R(Z)$ equations used in operational forecasting by the National Weather Service. Z is the equivalent reflectivity factor measured in $mm^6\ m^{-3}$ and R is the rainfall rate in $mm\ h^{-1}$.

R(Z) Equations	Rain Event Type
$Z = 300R^{1.4}$	Convective
$Z = 250R^{1.2}$	Tropical
$Z = 200R^{1.6}$	Summer Stratiform
$Z = 130R^{2.0}$	Winter Stratiform for Eastern USA
$Z = 75R^{2.0}$	Winter Stratiform for Western USA

1.4. Radar Coverage in Mid-Missouri

As mentioned in Chapter 1.2, rainfall rate equations rely on reflectivity values sensed by weather radars. In Columbia, MO (38.951 N, -92.327 W) there is a significant gap in coverage from NEXRAD that is maintained by the NWS (Ahrens and Henson 2016). NEXRAD is a network of 160 S-band Doppler radars that provide radar coverage to the continental United States. The two nearest NEXRAD radars from Columbia, MO are located in Kansas City, MO and St. Louis, MO which are over 130 km away (Figure 3). Therefore, MZZU was built at the South Farm Research Center (38.907 N, -92.268 W) as part of the NSF Established Program to Stimulate Competitive Research. The goal of this program was to fill this gap in radar coverage and to create a precipitation climatology for the region of Mid-Missouri.

MZZU scans horizontally in order to provide precipitation data to an area of over 15,000 km^2. In a vertical profile, MZZU uses different elevation angles to acquire data at set heights. The heights observed are determined by the elevation angle and the geographical distance of the precipitation from MZZU. Due to the curvature of the earth, precipitation data at longer ranges is retrieved at higher elevations in the atmosphere (Rinehart 2010). Since the elevation angles of MZZU are predetermined, there are also data gaps within the vertical profile. Thus, the MRR was installed at Bradford farm

(38.895 N, -92.206 W) to fill this vertical gap and obtain more accurate DSD profiles. The MRR is 5.608 km away from MZZU and has a maximum height range of 6200 m (Figure 4). In comparison, at this range the highest height observed by MZZU is 1957 m.

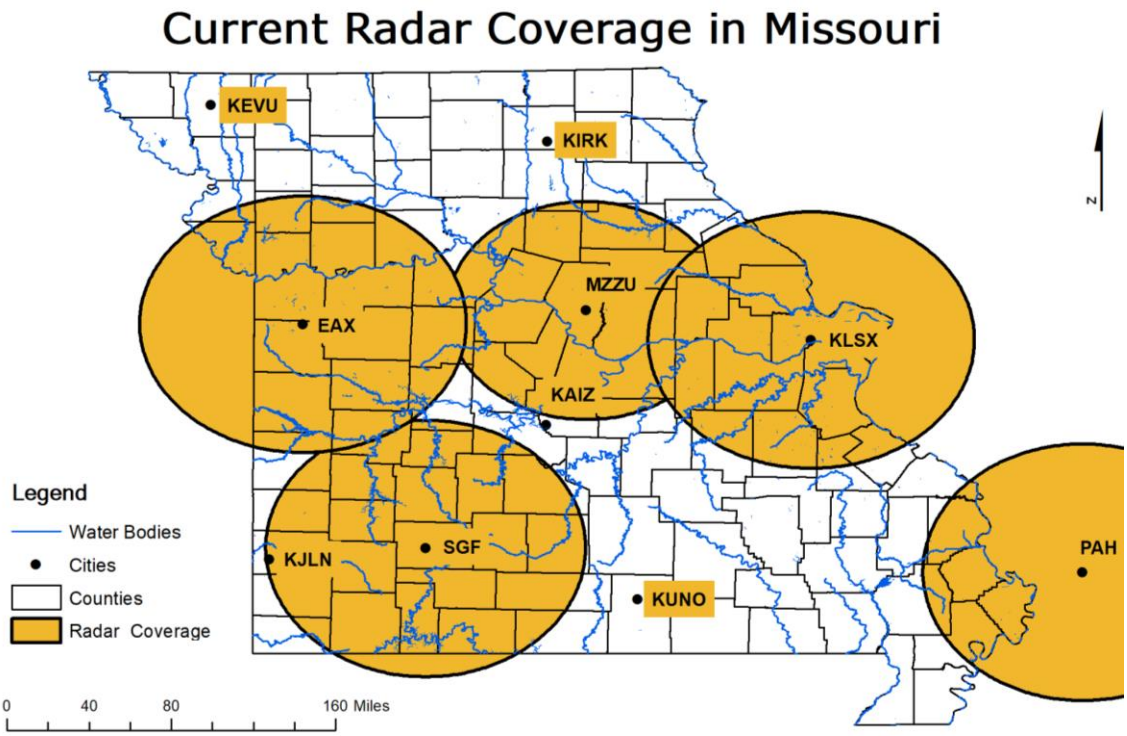

Figure 3. Map of current radar coverage in Missouri.

1.5. X-Band Limitations and Attenuation Correction

MZZU operates at a frequency of 9.35 GHz. This high frequency leads to extreme attenuation of Z in heavy rain events (Matrosov, et al. 2002). In 1990, a technique was developed that used the differential phase shift, ϕ_{dp}, to correct attenuated reflectivity values for X-band radars (Bringi, et al. 1990). This technique was then implemented by (Wen, Fox and Market 2020) to correct Z values obtained by MZZU:

$$Z_H^{att} = Z_H^{raw} + \alpha\left[\phi_{dp}(r) - \phi_{dp}(0)\right] \quad (5)$$

where Z_H^{att} is the attenuation corrected reflectivity, Z_H^{raw} is the base reflectivity, α is a constant given as 0.05 by Bringi et al. (1990), and ϕ_{dp} is the differential phase shift. Despite the attenuation correction, Z_H^{att}still underestimated the rainfall rate when compared to ground observations.

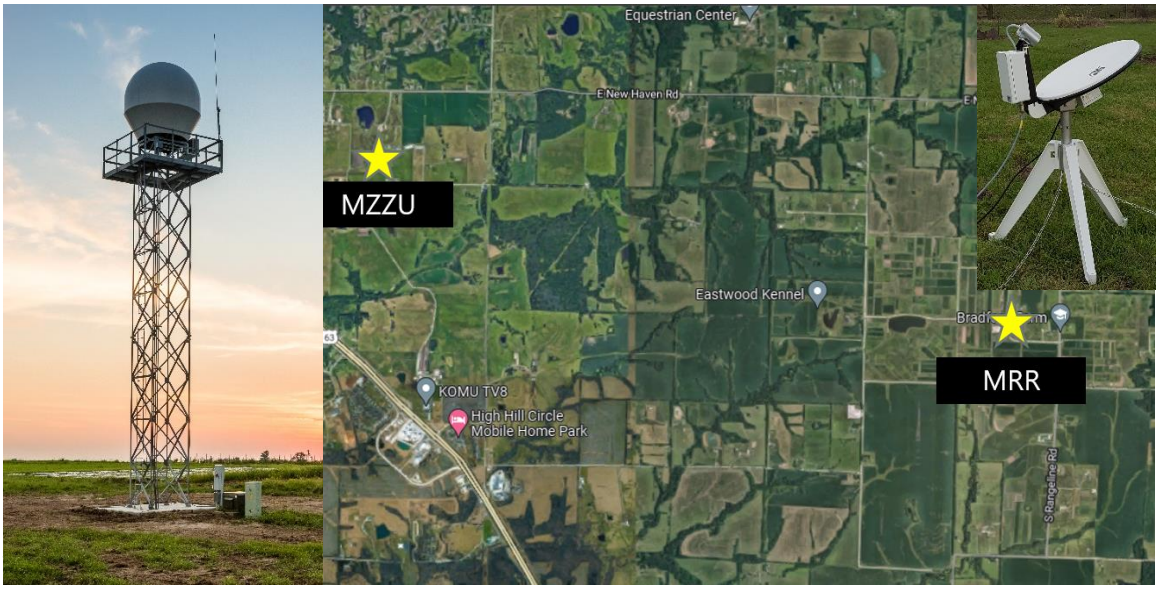

Figure 4. Map of the locations of MZZU and the MRR. Satellite imagery obtained from Google Maps.

Band radar located near Hamburg, Germany. First, they used the Path Integrated Attenuation algorithm from (Hitschfeld and Bordan 1953) to determine the expected attenuation of reflectivity in dBZ. This algorithm estimates the attenuation loss using the range in which the precipitation is monitored. Van Baelen, et al. used the expected attenuation to calibrate their radar and used the Marshall and Palmer equation, Eq. (2), to calculate the rain rate. The rain rate estimates from the X-Band radar were then compared to ground observations. In conclusion, the radar's performance varied from one event to the next. Therefore, the group proposed that future studies should develop new R(Z)

relationships based on event type. Van Baelen, et al. also suggested that MRR retrievals should be implemented in these new relationships to improve rain rate estimations.

(Lengfeld, Berenguer and Torres 2018) analyzed six different attenuation algorithms with four non-Doppler single polarized X-band radars in Northern Germany. They first used the algorithm outlined in (Hitschfeld and Bordan) as a base model. Three other algorithms used were developed by (Iguchi and Meneghini 1994). In (Iguchi and Meneghini), radar return echoes from the surface and mountain ranges were used to obtain a vertical profile of precipitation. This algorithm was developed to be used with satellite and airborne radar returns. (Lengfeld, Berenguer and Torres), substituted the returns from mountain ranges with overlapping data obtained by a C-Band radar in Hamburg, Germany. The other algorithms analyzed the relationship between reflectivity data retrieved from the X-Band and C-Band radars. An isotonic regression was performed on the ratio of reflectivity values from both radars (Lengfeld, et al. 2016) to develop the last algorithm. (Lengfeld, Berenguer and Torres 2018) concluded that the attenuation correction algorithms that used C-Band radar data resulted in better agreement of DSD variables with MRR observations.

(Reinoso-Rondinel and Schleiss 2021) evaluated the reliability of DSDs retrieved by MRRs. The study installed an MRR between an X-Band and C-Band radar in the Netherlands. The MRR retrieved DSD profiles for 15 events from November 2018 to February 2019. The study determined that MRR measurements can be used to calibrate weather radars. However, DSD profiles from the MRR should be analyzed first to eliminate impracticable values before they are used in calibration techniques.

2. DATA AND METHODS

2.1. MRR Data

The MRR operates within the K-Band at a frequency of 24 GHz, and its dish points up to capture DSDs in a vertical profile. The MRR detects the backscattered EM radiation from falling rain drops and uses the terminal fall velocity of the drops to calculate their diameters (METEK 2010). The drops sensed by the MRR are split into 32 height bins and 64 drop size bins. The height bins are determined by the gate length, which is 200m, and the size bins are determined by distribution of drop sizes that occur during the time of observation. Therefore, we can gather DSDs from heights of 200m to 6200m. The DSD profiles captured are then used to derive variables such as reflectivity, rain rate, and liquid water content. Reflectivity values were the only variable analyzed in this study.

2.2. MZZU Data

During the eight events analyzed, MZZU captured reflectivity values at eleven elevation angles. In order to obtain the reflectivity values that were sensed above the MRR, an algorithm in Python was developed. This algorithm used the geographical coordinates of the MRR to match the closest reflectivity value sensed by MZZU. To account for slantwise rain, the coordinates were shifted 250m north and the nearest reflectivity value was recorded. This shift was repeated seven more times every 45º, which resulted in nine total reflectivity values. All nine values were then averaged before comparison to the MRR.

2.3. MZZU and MRR Elevations

The first step in comparing reflectivity values from both sensors was to first match the elevations of the MRR gates to the MZZU beam heights. Using the equation presented in (Rinehart 2010):

$$H = \sqrt{R^2 + \left(\frac{4}{3}r_e\right)^2 + 2R\left(\frac{4}{3}r_e\right)\sin\varphi} - \frac{4}{3}r_e \quad (6)$$

the beam height of each elevation angle of MZZU can be calculated where H is the beam height, R is the range from the MRR, r_e is the radius of the earth, and φ is the elevation angle. The MRR gate heights are set by the gate length of 200 m which is determined within the METEK processing scheme. The heights from both sensors were analyzed to see which gates and elevation angles could be analyzed (Table 2). The MZZU beam height calculated from elevation angle 0.9˚ fell below any of the MRR gates, while the 5˚ angle was located in between gates. Therefore, these elevation angles from MZZU were not included in the study. The greatest elevation angle of 19º has a beam height of 1957m. Thus, MRR gates 2200-6200m were also emitted.

Table 2. Table of beam heights calculated using Eq. (5) for MZZU elevation angles. Column three provides the elevation of the matching MRR Gate for each elevation angle.

MZZU Elevation Angle	Beam Height (m)	MRR Gate Elevation (m)
0.9º	90	N/A
2º	198	200
3.5º	347	400
5º	496	N/A
6.5º	646	600
8º	799	800
10º	1003	1000
12º	1208	1200
14º	1418	1400
16º	1630	1600
19º	1957	2000

2.4. Time Formatting

An MZZU volume scan first begins at the lowest elevation angle and the radar antenna changes its angle as it rotates to capture data at all eleven elevations. The volume scan is then marked by the time in which the last elevation scan was complete. The temporal resolution of MZZU is highly variable due to the time it takes to switch from one elevation angle to another. On average a volume scan takes 3-5 minutes to complete. The MRR, however, processes spectral data every 10s. This data is then averaged every minute and stored within the data logger. Using the 1-minute averaged data, 3-minute and 5-minute averages were calculated in order to best match the temporal resolution of MZZU.

A function was developed to align the time variables from the MRR and MZZU scans. The function used the MRR time stamp to find the closest MZZU time stamp that corresponded with it. If the difference between the closest times was greater than 5 minutes, those MRR values were omitted from the analysis. The time stamps from the MRR indicate the start time for that specific averaging period. This is contrary to MZZU, which marks the time in which a volume scan was completed. Therefore, the MRR time stamps were shifted back one minute before they were matched to the MZZU. This process was repeated four times, the last time being a five-minute shift, to cover a full volume scan of MZZU.

2.5. Statistical Comparison

Once the elevations and times were aligned between both sensors, reflectivity values from the MRR were matched to the attenuated and attenuated corrected reflectivity values from the MZZU. The root mean square error (RMSE), coefficient of

determination (R^2), and the bias were calculated using the default statistical functions within (MATLAB 2019). A linear regression line was also fitted to each comparison and the slope coefficient of the line was recorded. This statistical analysis of correlation within the reflectivity values were conducted at nine elevations for eight different events.

2.6. Case Studies

The case studies were selected based on days in which more than 6 mm of rain fell within 24 hours. Days within the above criteria were then filtered to find events in which both MZZU and the MRR were operational. Eight events were then selected that consisted of five convective events and three stratiform events. Event type was determined by reflectivity values received by MZZU (Figure 2). A brief summary of the events can be found in (Table 3).

Table 3. Description of the eight events analyzed in the study. R_{total} is the total accumulated rainfall and R_{max} is the maximum recorded rainfall collected in one hour. The minutes refers to the number of matching pairs within the one-minute data. Rain rate data was captured by the rain gauge located at Bradford Farm.

Event	Date	Type	R_{total} (mm)	R_{max} (mm hr^{-1})	Minutes
1	17 July 2019	Convective	9.91	9.91	24
2	11 August 2019	Convective	22.10	16.51	155
3	27 August 2019	Convective	14.99	13.46	102
4	30 August 2019	Stratiform	38.61	12.45	602
5	8 September 2019	Convective	19.30	10.92	240
6	10 January 2020	Stratiform	51.56	7.11	134
7	25 May 2020	Convective	6.60	4.06	49
8	9 June 2020	Stratiform	68.83	17.27	562

3. RESULTS

3.1. Averaging Scheme and Time Shift

As mentioned in Chapter 2.4, different averaging schemes and time shifts were applied to the MRR data before it was correlated with MZZU. In Table 4, the statistical values are present for the three different averaging schemes for all matching pairs in the eight events. The statistical values are calculated from MZZU's attenuated corrected reflectivity, but conclusions apply to both corrected and noncorrected values (Table 4). The 5-minute averaging scheme resulted in the highest R^2 values among all elevation levels with the average value of 0.77. The 3-minute averaging scheme generated R^2 values greater than 0.7; however, RMSE values in the 5-minute data were lower at all levels. The 1-minute averaging scheme was the least correlated with the MZZU, which is likely a result of the variability of DSD retrievals from the MRR.

Table 4. Statistical values using three different averaging schemes. The comparison analyzed is between the MRR reflectivity and the attenuated correct reflectivity from MZZU. RMSE and bias are in units of dBZ, and the angle refers to the elevation angle of MZZU.

	1 Minute Average			3 Minute Average			5 Minute Average		
Angle	RMSE	R^2	Bias	RMSE	R^2	Bias	RMSE	R^2	Bias
2˚	6.58	0.60	8.13	5.36	0.72	8.08	5.17	0.77	8.21
3.5˚	6.93	0.53	7.91	5.87	0.64	7.68	5.60	0.71	7.90
6.5˚	6.07	0.62	7.39	4.96	0.74	7.18	4.94	0.77	7.37
8˚	6.46	0.60	7.22	5.13	0.73	7.13	4.63	0.81	7.29
10˚	6.12	0.61	7.18	5.04	0.73	7.12	4.53	0.81	7.21
12˚	5.65	0.69	7.30	4.69	0.79	7.26	4.76	0.81	7.31
14˚	6.15	0.63	6.94	5.15	0.74	6.95	4.82	0.80	6.94
16˚	5.98	0.64	6.94	5.60	0.68	6.81	5.14	0.77	7.10
19˚	6.81	0.55	6.41	6.73	0.55	6.22	6.48	0.65	6.67

Using the 5-minute averaging scheme as our basis, the five separate time shifts were evaluated to determine which time shift aligned the data the best. Shifting the MRR time back one minute resulted in the best fit for the first five elevations. The last four

elevations had the highest correlation with no time shift applied. This coheres to MZZU's temporal resolution where the higher elevations scans will occur closer to MRR time stamps. The time shift specifically helps to align start and stop times of rainfall during these events (Figure 5).

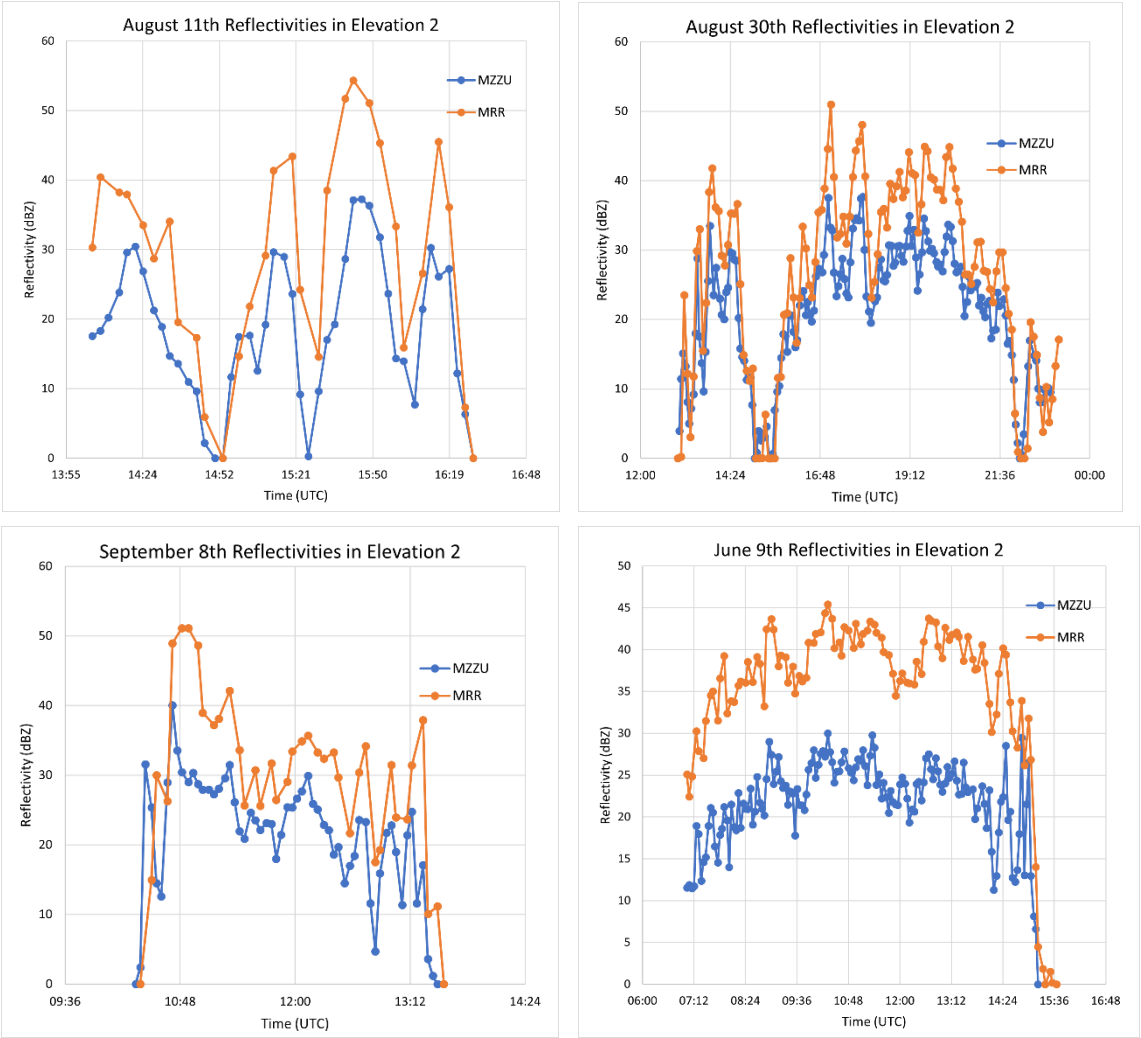

Figure 5. Reflectivity from MZZU (blue) and MRR (orange) during four events; August 11th, 2019 (Top Left), August 30th, 2019 (Top Right), September 8th, 2019 (Bottom Left), and June 9th, 2020 (Bottom Right). The MRR timestamps were shifted back by one minute and reflectivity is plotted from the 2º elevation angle.

3.2. Attenuation Correction

Once the appropriate averaging scheme and time shift were applied to the MRR reflectivity values, the data was correlated with MZZU. First, an analysis was done between the base reflectivity, Z_{base}, and the attenuated reflectivity, Z_{ac}, from MZZU (Table 5). The correlation of Z_{base} resulted in higher values of R^2 at all elevations when compared to Z_{ac}. This relationship contradicts the hypothesis which assumes that Z_{ac} is more accurate than Z_{base}. This could be a result of the unfiltered values in the MRR data.

Negative values of reflectivity are both present in the MRR data and the uncorrected reflectivity from MZZU. These points result in a tight correlation in values less than 0 dBZ (Figure 6). The attenuation correction algorithm replaces most of the negative values in the MZZU data with zeros. The negative reflectivity values from the MRR were left uncorrected. Therefore, the statistical values for the Z_{base} include more negative values that match with the negative values of the MRR. However, negative reflectivity values occur when there is no precipitation present. Therefore, the statistical analysis of Z_{ac} provides a better representation of the correlation between MZZU and the MRR in rain environments. Nevertheless, a process should be developed to filter out nonrealistic values from the MRR data to confirm this statement.

3.3. MZZU and MRR Reflectivity Analysis

Now using Z_{ac}, the reflectivity values captured from MZZU were compared to the MRR data. The average R^2 value among all elevations in all eight events was 0.79. The highest R^2 values were evaluated in elevations 4, 5, and 6. The performance dwindled as the elevation increased higher into atmosphere T. The average bias calculated was 7.71 dBZ and indicates that MZZU is underfitting in comparison to the MRR. The linear

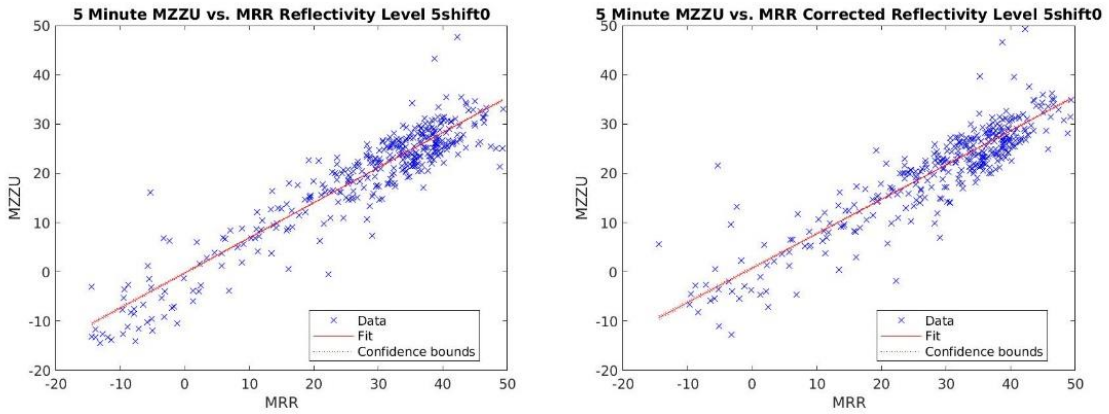

Figure 6. Scatterplots of MZZU and MRR reflectivity at the 8˚ elevation angle. The left plot uses the base reflectivity and the right uses attenuated corrected reflectivity

regression lines show good linear fits between the two datasets. The slopes of the regression lines range from 0.61 to 0.71. This analysis suggests that the MZZU attenuation correction algorithm consistently underestimates reflectivity values in all nine elevations (Figure 7). This linear relationship between MZZU and the MRR could be exploited to further improve and calibrate Z_{ac} values. If the linear relationship is assumed to exist in all events, the average bias of 7.71dBZ could act as a correction for Z_{ac} among a constant slope between 0.61 and 0.71.

Table 5. Statistical values for both the base reflectivity, Z_{base}, and the attenuated corrected reflectivity, Z_{ac}, from MZZU. The reflectivity data is correlated with the 5-minute averaging scheme data from the MRR with a 1-minute shift in the first five angles. RMSE and bias are in units of dBZ and the angle refers to the elevation angle of MZZU.

	Z_{base}			Z_{ac}		
Angle	RMSE	R^2	Bias	RMSE	R^2	Bias
2˚	4.72	0.83	8.73	4.45	0.82	8.20
3.5˚	4.86	0.82	8.28	4.80	0.77	7.79
6.5˚	4.13	0.86	7.77	3.99	0.84	7.31
8˚	4.02	0.87	7.62	4.12	0.84	7.19
10˚	3.99	0.87	7.55	4.09	0.83	7.14
12˚	4.43	0.85	7.74	4.76	0.81	7.31
14˚	4.48	0.85	7.38	4.82	0.80	6.94
16˚	4.91	0.80	7.31	5.14	0.77	7.10
19˚	6.07	0.72	7.09	6.48	0.65	6.67

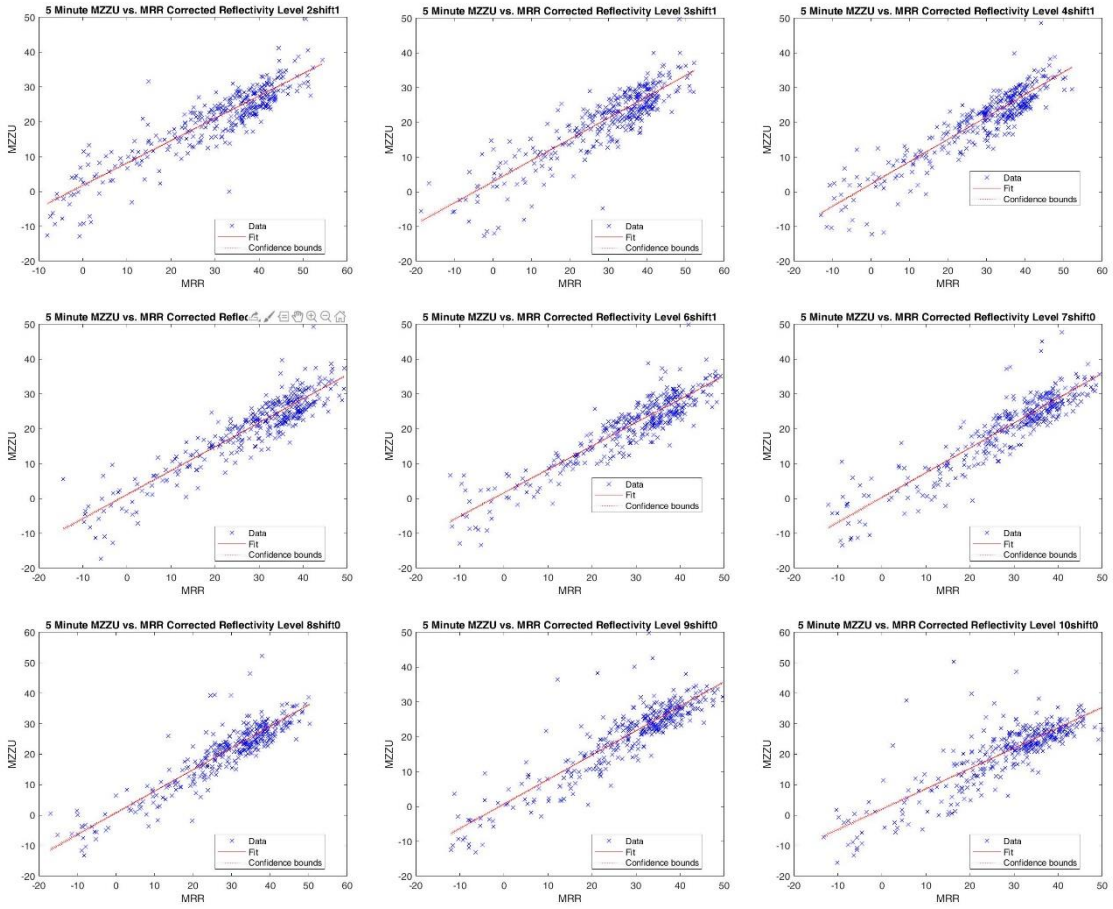

Figure 7. Scatterplots of MZZU and MRR reflectivity at nine elevations. The linear regression line is fitted to each plot (red).

3.4. Event Analysis

The statistical values in (Table 5) provide feedback to the performance of MZZU during all events evaluated. Further analysis evaluated the DSD profiles in each of the eight different events. As described in (Table 3), we can broadly label each rain event as stratiform or convective based on reflectivity values observed in the events. In order to compare these two event types, the time averaging scheme described in Chapter 2.4 had to be changed for each event. This is because of MZZU's continuous scanning mechanism that results in sporadic volume scan times that change each day. Another issue encountered during convective rain events was the short time durations. When

using the 5-minute averaging scheme in these events, a very small number of points were analyzed. This decrease in the total number of comparisons led to extreme values of RMSE greater than 10 dBZ. Event 5 was the longest lasting convective rain event, which took place over the course of three hours. Therefore, a 3-minute averaging scheme was employed on the MRR data with multiple time shifts for each elevation. The statistical analysis for Event 5 was compared to Event 8 (Table 6). Event 8 was a stratiform rain event that lasted over eight hours, so the 5-minute averaging scheme was used.

Table 6. Statistical values from September 8th, 2019 (Event5) and June 9th, 2020 (Event 8). Attenuated reflectivity from the MZZU is correlated to the reflectivity values from the MRR. RMSE and bias are in units of dBZ and the angle refers to the elevation angle of MZZU.

	Event 5				Event 8			
Angle	RMSE	R^2	Bias	Slope	RMSE	R^2	Bias	Slope
2˚	5.18	0.81	7.28	0.69	2.27	0.92	13.60	0.81
3.5˚	5.09	0.79	6.35	0.60	2.42	0.91	13.14	0.85
6.5˚	4.97	0.78	5.58	0.59	2.47	0.90	12.27	0.80
8˚	4.50	0.81	5.58	0.64	2.45	0.92	11.84	0.79
10˚	4.34	0.82	4.75	0.62	2.35	0.92	11.65	0.77
12˚	3.60	0.87	4.63	0.62	2.52	0.91	11.02	0.77
14˚	3.44	0.91	4.49	0.74	2.35	0.91	10.73	0.68
16˚	2.75	0.93	4.12	0.70	2.01	0.94	10.66	0.74
19˚	6.65	0.68	2.64	0.64	2.61	0.90	10.21	0.76

Attenuated reflectivity from MZZU correlated much better with the MRR during stratiform rain events (Figure 8). R^2 values were greater than 0.9 in all elevations with very low RMSE values during Event 8. The average bias was 11.68 dBZ among all elevations. The convective rain events resulted in lower R^2 values and higher RMSE. However, the bias was nearly half as large as those found in the stratiform rain events (Figure 9). Despite a better correlation to the MRR data, stratiform rain events underestimated Z_{ac} more than convective rain events. This could likely be a result of radome attenuation. Radome attenuation occurs when a thin layer of water covers the

radome that results in power loss in the EM waves (Frasier, et al. 2013). The radome remains covered for longer periods of time in stratiform rain events. Therefore, a greater attenuation can be expected in these events. The statements above complicate the linear relationship described in Chapter 3.3. The linear relationship changes drastically from one event to another. Thus, calibrations would have to change based on event type to acquire the best correlation between the MRR and the MZZU. Another solution would be to apply a less rigorous calibration for all events and tackle the effect of radome attenuation in a separate study.

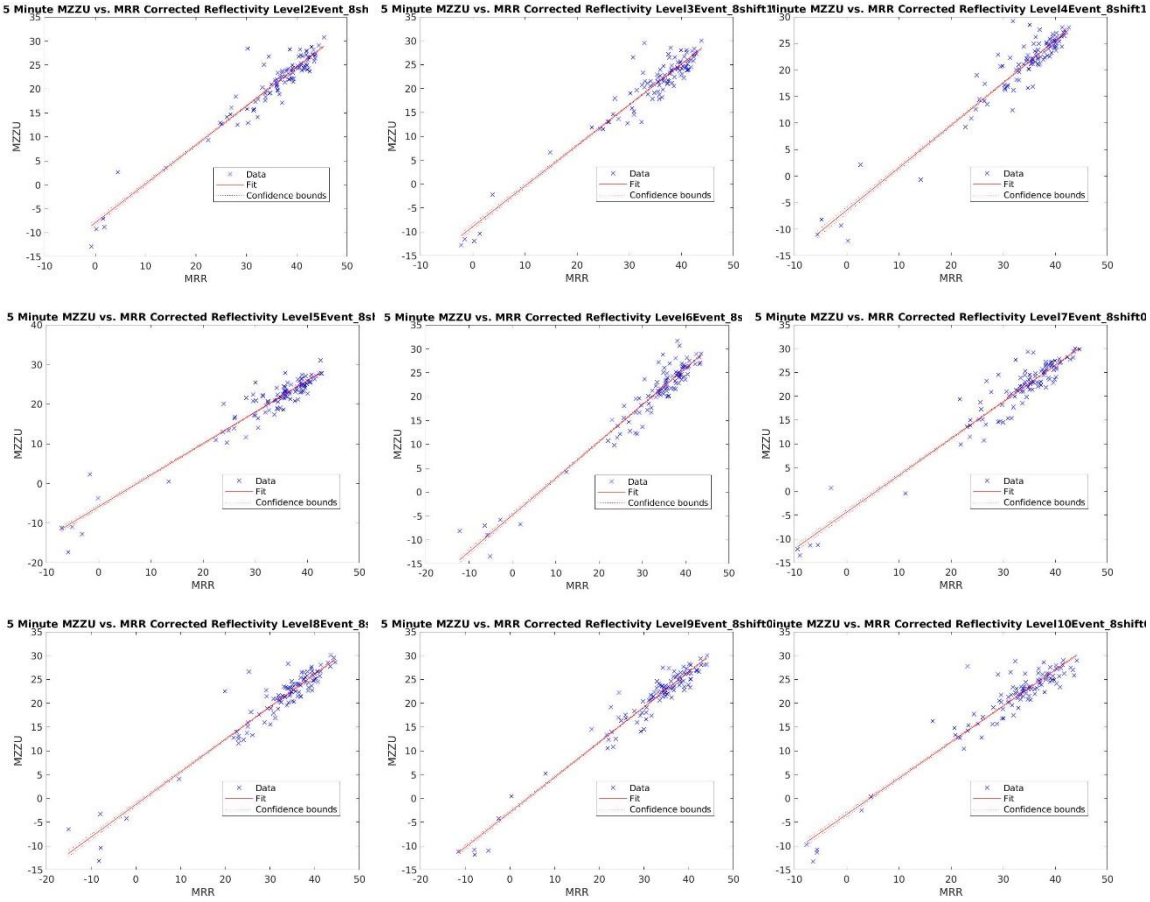

Figure 8. Scatterplots of MZZU and MRR reflectivity at nine elevations on June 9th, 2020. The linear regression line is fitted to each plot (red).

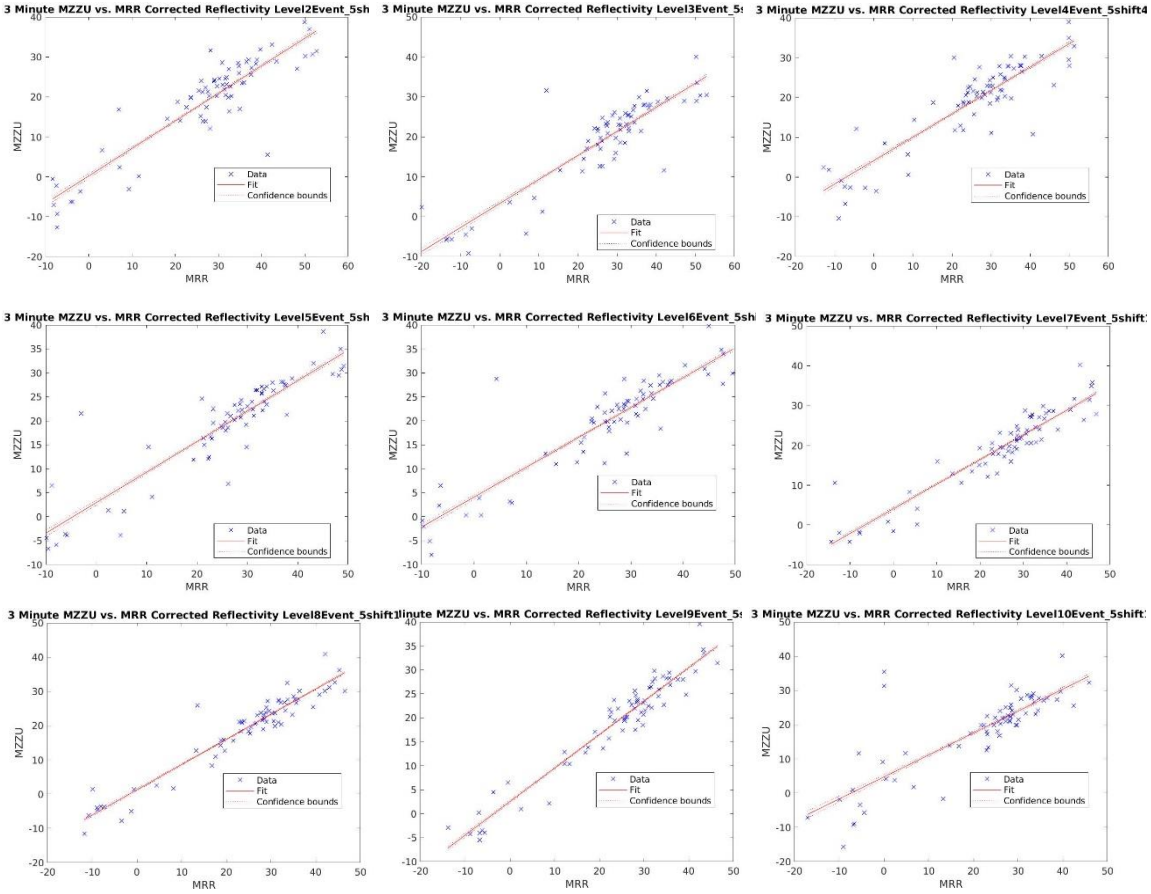

Figure 9. Scatterplots of MZZU and MRR reflectivity at nine elevations on September 8th, 2019. The linear regression line is fitted to each plot (red).

4. CONCLUSIONS

Weather Radars use electromagnetic waves to sense rain and to measure drop size distributions. These DSDs are used to create quantitative precipitation estimates in order to forecast rainfall rates. Due to a gap in radar coverage, a X-band dual-polarization Doppler radar (MZZU) was installed in Mid-Missouri. X-Band radars attenuate in heavy rain events; therefore, attenuation correction algorithms have been developed to improve accuracy. In 2020, (Wen, Fox and Market) used one of the algorithms to correct MZZU data. This study uses a K-band vertical pointed microwave rain radar (MRR), to assess the accuracy of attenuated correct reflectivity values captured by MZZU.

When analyzing the correlations of base reflectivity, Z_{base}, and attenuated reflectivity, Z_{ac}, from MZZU, it was found that the Z_{base} had a better correlation to the MRR data in the eight events studied. This is theorized to be an effect of unfiltered MRR data. Therefore, a processing scheme to omit nonrealistic DSD values from the MRR should be developed. The correlation in all matching pairs between Z_{ac} from MZZU and reflectivity values from the MRR resulted in R^2 values greater than 0.75 with an average negative bias of 7.71 dBZ. Thus, the Z_{ac} values from MZZU are underestimating reflectivity. In stratiform rain events, R^2 increased to values greater than 0.9. The bias in these events, however, decreased further to an average of negative 11.68 dBZ. This suggests that MZZU underestimates reflectivity more during stratiform rain events. The linear regression slope values typically ranged between 0.6 and 0.8 in all events. By using the biases and the slopes found in the correlation analysis, a calibration method can be developed to further improve Z_{ac} values calculated from MZZU.

Future studies should first focus on filtering DSD values that are currently sensed by the MRR at Bradford Farm. Once this filtering is done, more derived products can be analyzed, such as differential reflectivity, rainfall rate, and liquid water content. The criteria for case studies should be widened to try and capture more events where both sensors are operational. Another suggestion is to move the MRR to a different range from MZZU. This change would determine if the linear relationship observed in the regression model is similar at different ranges. Then by using MRR data a correction tool, Z_{ac} can be calibrated to improve accuracy.

In conclusion, the attenuation corrected reflectivity from MZZU data underestimates reflectivity values when compared to the MRR. The reflectivity values from the MRR provide an opportunity to further calibrate Z_{ac} by using the linear relationship observed between the two sensors. This calibration would improve the accuracy of reflectivity values from MZZU, which then would result in better rainfall rate estimates for Mid-Missouri.

BIBLIOGRAPHY

Ahrens, C. D., and R. Henson. 2016. *Meteorology Today Eleventh Edition.* Boston: Cengage Solutions.

Ashley, Sharon T., and Walker S. Ashley. 2008. "Flood Fatalities in the United States." *Journal of Applied Meteorology and Climatology* 805-818.

Bringi, V.N., V. Chandrasekar, N. Balakrishnan, and D.S. Zrnic. 1990. "An Examination of Propagation Effects in Rainfall on Radar Measurements at Microwave Frequencies." *American Meteorological Society* 829-840.

Frasier, Stephen J., Fadela Kabeche, Jordi Figueras i. Ventura, Hassan Al-Sakka, and Pierre Tabary. 2013. "In-Place Estimation of Wet Radome Attenuation at X Band." *Journal of Atmospheric and Oceanic Technology* 917-928.

Google. 2022. *Columbia, Missouri.* Accessed November 30, 2022. https://www.google.com/maps.

GR2Analyst. 2022. *version 2.93.* Suwanee, Georgia: Gibson Ridge Software, LLC.

Hitschfeld, W., and J. Bordan. 1953. "Errors inherent in the radar measurements of rainfall at attenuation wavelengths." *Journal of Meteorology* 58-67.

Iguchi, T., and R. Meneghini. 1994. "Intercomparison of Single-Frequency Methods for Retrieving a Vertical Rain Profile from Airborne or Spaceborne Radar Data." *Journal of Atmospheric and Oceanic Technology* 1507-1516.

Lengfeld, K, M. Clemens, C. Merker, H. Munster, and F. Ament. 2016. "A Simple Method for Attenuation Correction in Local X-Band Radar Measurements Using

C-Band Radar Data." *Journal of Atmospheric and Oceanic Technology* 2315-2329.

Lengfeld, K., M. Berenguer, and D. S. Torres. 2018. "Intercomparison of attenuation correction algorithms for single-polarized X-band radars." *Atmospheric Research* 116-132.

Marshall, J. S., and W. M. Palmer. 1948. "The size distribution of raindrops." *Journal of Atmospheric Sciences* 165-166.

MATLAB. 2019. *version 9.7.0 (R2019b).* Natick, Massachusetts: The MathWorks Inc.

Matrosov, S. Y., K. A. Clark, B. E. Martner, and A. Tokay. 2002. "X-band polarimetric radar measurements of rainfall." *Journal of Applied Meteorology* 941-952.

METEK. 2010. "MRR Physical Basics version 5.2.0.9." Meteorologische Messtechnik GmbH. 4-10.

Peters, G., Fischer B., H. Munster, M. Clemens, and A. Wagne. 2005. "Profiles of raindrop size distributions as retrieved by Micro Rain Radars." (Journal of Applied Meteorology) 44 (12): 1930-1949.

Rauber, Robert M., John E. Walsh, and Donna J. Charlevoix. 2017. *Severe and Hazardous Weather 5th Edition.* Dubuque: Kendall Hunt Publishing Company.

Reinoso-Rondinel, Ricardo, and Marc Schleiss. 2021. "Quantitative Evaluation of Polarimetric Estimates from Scanning Weather Radars Using a Vertically Pointing Micro Rain Radar." *Journal of Atmospheric and Oceanic Technology* 481-499.

Rinehart, Ronald E. 2010. *Radar for Meteorologists 5th Edition.* Columbia: Rinehart Publications.

Ryzhkov, Alexander V, and Dusan S Zrnic. 2019. *Radar Polarimetry for Weather Observations.* Cham: Springer.

Schuur, T.J., A. V. Ryzhkov, and D.R. Clabo. 2005. "Climatological analysis of DSDs in Oklahoma as revealed by 2D-video disdrometer and polarimetric WSR-88D." *32nd Conference on Radar Meteorology.*

Van Baelen, J., Y. Pointin, W Wobrock, A. Flossmann, G. Peters, F. Tridon, and C. Planche. 2009. "Precipitation and microphysical studies with a low cost high resolution X-band radar: an innovative project prospective." *Advances in Geosciences* 25-32.

Wen, Guang, Neil I. Fox, and Patrick S. Market. 2020. "The Quality Control and Rain Rate Estimation for the X-Band Dual-Polarization Radar: A Study of Propagation of Uncertainty." *Remote Sensing* 12 (1072): 1-28. doi:10.3390/rs12071072.